Development of multi time-step tomographic reconstruction with RAVEN

Yoshito Ono[a], Masayuki Akiyama[a], Shin Oya[b], and Olivier Ladière[c]

[a]Astronomical Institute, Tohoku University, 6-3 Aramaki, Aoba-ku, Sendai 980-8578, Japan
[b]TMT-J Project Office, NAOJ, 2-21-1 Osawa, Mitaka, Tokyo 181-8588, Japan
[c]NRC-Herzberg, 5071 West Saanich Rd., Victoria, British Columbia, Canada

ABSTRACT

In this paper, we present a tomographic reconstruction method to reduce a tomographic error, *multi time-step reconstruction*, for a wide-field adaptive optics (WFAO). Based on the frozen flow assumption, we can compute the time evolution of measurements from wave-front sensors (WFS) at previous time-steps with using wind information. Our idea is to reduce the tomographic error by using the measurements at both the current and previous time-steps simultaneously. We also develop a method to estimate wind speed and direction at each altitude from temporal correlations of phase distortion pattern reconstructed by a classical tomography. We evaluate the performance of the method by a laboratory experiment with the RAVEN, a multi-object adaptive optics (MOAO) technical and science demonstrator. In the laboratory experiment, our wind estimation method can estimate wind speeds and directions of multiple layers. By the multi time-step reconstruction method, the ensquared energy in a 140 mas box increases about 3–5% compared with a classical tomographic reconstruction.

Keywords:

1. INTRODUCTION

Classical single-conjugate adaptive optics (SCAO) systems have a critical limitation that the correction of SCAO is effective only within a limited angle at a time. Two wide-field AO (WFAO) concepts, involving tomographic wave-front reconstruction to estimate the atmospheric volume with using multiple guide stars, come out from requirements to apply AO correction into wide field simultaneously and to increase the efficiency of AO assisted observations: multi-conjugate adaptive optics (MCAO)[1] and multi-object adaptive optics (MOAO).[2] MCAO compensates for the phase distortion three-dimensionally by multiple DMs, which are put in series and conjugated at different heights in the atmosphere, and provides a uniform correction over a wide field of view (FoV). MOAO has several science paths each containing a DM and provides the optimized correction simultaneously for multiple small patches in the wide field of regard (FoR).

The key parameters of WFAO systems are the performance of AO correction and the FoR size. For example, in a MOAO case, to utilize the multiplicity for the high redshift galaxies with low number density, a wide FoR is necessary to find the multiple science targets in the FoR. These parameters depends strongly on the accuracy of the tomographic wave-front reconstruction. The one of the limitation of the tomographic wave-front reconstruction is the limited number of GS. From the limited number of GSs, we can not get sufficient information of the phase distortion in a volume of the atmosphere corresponding to the FoR. For example, the area on the atmospheric turbulence layers,which is not covered by the optical path of the GS, causes a significant tomographic error because there is no information about this area in the measurements of wave-front sensors (WFSs). We referred to this area as a *uncovered area*. The area covered only by an optical path of one GS also results in the tomographic error. This area is referred to as a *unoverlapped area*. The WFSs probes the integrated phase distortion in its GS direction. In other words, the phase distortions from multiple turbulence layers are degenerated in the WFS measurement. In order to solve this degeneracy and to reconstruct the phase

Further author information: (Send correspondence to A.A.A.)
A.A.A.: E-mail: aaa@tbk2.edu, Telephone: 1 505 123 1234
B.B.A.: E-mail: bba@cmp.com, Telephone: +33 (0)1 98 76 54 32

distortion on each atmospheric turbulence layer by the tomographic wave-front reconstruction, the information from multiple directions is necessary, that is, all areas should be covered by two or more GS optical paths. We can not solve the degeneracy for the *unoverlapped area*.

In this paper, we develop an algorithm of the tomographic wave-front reconstruction, which reduces the tomographic error due to the lack of information and to extend the size of FoR of WFAO systems without reducing the AO performance. Also, we present the method to estimate wind speeds and directions at multiple altitudes, which is essential for the new tomography algorithm. The basic idea of our algorithm is to solve the tomographic wave-front reconstruction by using measurement from multi time-steps based on the frozen flow assumption.

2. METHOD

2.1 Multi Time-Step Reconstruction

We consider the tomographic reconstruction for the case of a MOAO with N_{gs} GSs, in which the direction of j-th GS are denoted as $\boldsymbol{\alpha_j} = (\alpha_{jx}, \alpha_{jy})$. There are N_{layer} turbulence layers at different altitudes. The phase distortion of the aperture-plane wave-front $\varphi_{\boldsymbol{\theta}}(\boldsymbol{x}, t)$ in the direction $\boldsymbol{\theta}$ at time t is represented as the sum of the phase distortion caused by the turbulence layers,

$$\varphi_{\boldsymbol{\theta}}(\boldsymbol{x}, t) = \sum_{i=1}^{N_{\mathrm{layer}}} \phi_i(\boldsymbol{x} + h_i\boldsymbol{\theta}, t), \tag{1}$$

where $\boldsymbol{x} = (x, y)$ is a vector of a two-dimensional spatial coordinate, h_i is an altitude of i-th turbulence layer, and $\phi(\boldsymbol{x}, t)$ is a phase distortion at a point $\boldsymbol{x}$ on i-th turbulence screen at time t. We define a ray-tracing matrix $\boldsymbol{P_\theta^i}$, which extracts phase distortion within a optical path footprint in the direction $\boldsymbol{\theta}$ from i-th atmospheric turbulence by using a bilinear interpolation. Using the ray-tracing matrix, Eq. (1) is rewritten with considering all phase points in the aperture as

$$\boldsymbol{\varphi_\theta}(t) = \sum_{i=1}^{N_{\mathrm{layer}}} \boldsymbol{P_\theta^i \phi_i}(t) = \boldsymbol{P_\theta \phi}(t), \tag{2}$$

where $\boldsymbol{\varphi_\theta}$ is a column vector containing the phase values of the wave-front propagating from direction θ and $\boldsymbol{\phi}$ is a column vector of phase distortions on a discrete grid on the i-th turbulence layer.

In MOAO system, a tomographic reconstructor for a science target in direction $\boldsymbol{\beta}$ is determined to minimize the residual phase variance[3] as

$$\boldsymbol{E_\beta} = \underset{\boldsymbol{E_\beta}}{\mathrm{argmin}} \langle ||\boldsymbol{\varphi_\beta} - \hat{\boldsymbol{\varphi}}_{\boldsymbol{\beta}}||^2 \rangle. \tag{3}$$

where $\boldsymbol{E_\beta}$ is the tomographic reconstructor for the direction $\boldsymbol{\beta}$, $\boldsymbol{\varphi_\beta}$ is the actual aperture-plane phase coming from the direction $\boldsymbol{\beta}$, $\hat{\boldsymbol{\varphi}}_{\boldsymbol{\beta}}$ is the aperture-plane phase reconstructed by the tomographic reconstruction, and $\langle\rangle$ indicates ensemble average over time. This reconstructor is known as *minimum variance reconstructor*,[4] which provides the solution to minimize the variance of the residual phase at the aperture-plane.

We assume using multiple Shack-Hartmann WFSs (SH-WFSs). The slope vector, $\boldsymbol{s_\alpha}(t)$, which contains the slope of all SH-WFSs at time t, is defined as

$$\boldsymbol{s_\alpha}(t) = \boldsymbol{\Gamma_\alpha P_\alpha \phi}(t) + \boldsymbol{\eta}(t), \tag{4}$$

where $\boldsymbol{\Gamma_\alpha}$ is a discrete phase-to-slope operator which converts phases into slopes, $\boldsymbol{P_\alpha}$ is a ray tracing matrix for the directions of all N_{gs} GSs, and $\boldsymbol{\eta_\alpha}(t)$ is a column vector of the noise in measurements of all SH-WFSs. We use Fried geometry to define $\boldsymbol{\Gamma_\alpha}$.

With Eq. (4) and $\hat{\boldsymbol{\varphi}}_{\boldsymbol{\beta}}(t) = \boldsymbol{E_\beta s_\alpha}(t)$, the minimum variance reconstructor can be given as

$$\boldsymbol{E_\beta} = \boldsymbol{P_\beta}(\boldsymbol{P_\alpha^T \Gamma_\alpha^T \Sigma_{\eta\eta}^{-1} \Gamma_\alpha P_\alpha} + \boldsymbol{\Sigma_{\phi\phi}^{-1}})^{-1} \boldsymbol{P_\alpha^T \Gamma_\alpha^T \Sigma_{\eta\eta}^{-1}} \tag{5}$$

where $\boldsymbol{\Sigma_{\eta\eta}}$ is a noise covariance matrix and $\boldsymbol{\Sigma_{\phi\phi}}$ is a covariance matrix of the phase distortion of the atmospheric turbulence. The computation efficiency for the tomographic reconstruction is a critical issue for the ELT-scale WFAO systems. An efficient sparse matrix computation is proposed[4] to solve this issue since the matrices composing the $\boldsymbol{E_\beta}$ are sparse matrices, except for the inverse of the phase covariance matrix, $\boldsymbol{\Sigma_{\phi\phi}^{-1}}$. Therefore, we use a sparse matrix approximation for the inverse of the phase covariance matrix by using a discrete laplacian matrix, $\boldsymbol{L}$, that is, $\boldsymbol{\Sigma_{\phi\phi}^{-1}} = \boldsymbol{L^T L}$.[4] The scaling of the $\boldsymbol{L}$ is described in.[5] Then, the final formula is given as

$$\boldsymbol{E_\beta} = \boldsymbol{P_\beta}(\boldsymbol{P_\alpha^T \Gamma_\alpha^T \Sigma_{\eta\eta}^{-1} \Gamma_\alpha P_\alpha} + \boldsymbol{L^T L})^{-1} \boldsymbol{P_\alpha^T \Gamma_\alpha^T \Sigma_{\eta\eta}^{-1}} \tag{6}$$

This is classical tomographic reconstructor. In this paper, we refer to this reconstructor as the single time-step reconstructor.

Under the assumption of the frozen flow, the temporal evolution of the turbulence layer within a time of Δt can be consider as the shift due to the wind as

$$\phi(\boldsymbol{x}, t - \Delta t) = \phi(\boldsymbol{x} + \boldsymbol{v}\Delta t, t), \tag{7}$$

where $\boldsymbol{v} = (v_x, v_y)$ is a wind speed at the altitude of the turbulence layer. By using this equation, the relation between the phase distortion at the current time-step and the measurements at the previous time-step is given as

$$\boldsymbol{s_\alpha}(t - \Delta t) = \boldsymbol{\Gamma_\alpha P_\alpha^{\Delta t}} \boldsymbol{\phi}(t) + \boldsymbol{\eta}(t - \Delta t), \tag{8}$$

where $\boldsymbol{P_\alpha^{\Delta t}}$ is a ray tracing matrix taking into account of the shift due to the wind within Δt. In order to use the measurements from both of the current and previous time-steps simultaneously to increase information and to improve the performance of the tomography, the final measurement model is a concatenation of Eq. (4) and Eq. (8). The reconstructor can be given as well as the single time-step reconstructor.

$$\tilde{\boldsymbol{E}}_{\boldsymbol{\beta(\Delta t)}} = (\tilde{\boldsymbol{P}}^T_{\boldsymbol{\alpha(\Delta t)}} \tilde{\boldsymbol{\Gamma}}^T_{\boldsymbol{\alpha(\Delta t)}} \tilde{\boldsymbol{\Sigma}}^{-1}_{\boldsymbol{\eta\eta(\Delta t)}} \tilde{\boldsymbol{\Gamma}}_{\boldsymbol{\alpha(\Delta t)}} \tilde{\boldsymbol{P}}_{\boldsymbol{\alpha(\Delta t)}} + \boldsymbol{L^T L})^{-1} \tilde{\boldsymbol{P}}^T_{\boldsymbol{\alpha(\Delta t)}} \tilde{\boldsymbol{\Gamma}}^T_{\boldsymbol{\alpha(\Delta t)}} \tilde{\boldsymbol{\Sigma}}^{-1}_{\boldsymbol{\eta\eta(\Delta t)}} \tag{9}$$

where

$$\tilde{\boldsymbol{P}}_{\boldsymbol{\alpha(\Delta t)}} = \begin{bmatrix} \boldsymbol{P_\alpha} \\ \boldsymbol{P_\alpha^{\Delta t}} \end{bmatrix}, \quad \tilde{\boldsymbol{\Gamma}}_{\boldsymbol{\alpha(\Delta t)}} = \begin{bmatrix} \boldsymbol{\Gamma_\alpha} & \boldsymbol{0} \\ \boldsymbol{0} & \boldsymbol{\Gamma_\alpha} \end{bmatrix}, \quad \tilde{\boldsymbol{\Sigma}}_{\boldsymbol{\eta(\Delta t)}} = \begin{bmatrix} \boldsymbol{\Sigma_{\eta\eta}} & \boldsymbol{0} \\ \boldsymbol{0} & \boldsymbol{\Sigma_{\eta\eta}} \end{bmatrix}. \tag{10}$$

2.2 Wind Estimation

The phase distortion of the turbulence layer at each altitude can be reconstructed with using a part of the tomographic reconstructor from the slopes,

$$\begin{bmatrix} \hat{\boldsymbol{\phi}}_{\boldsymbol{1}}(t) \\ \vdots \\ \hat{\boldsymbol{\phi}}_{\boldsymbol{N_{\text{layer}}}}(t) \end{bmatrix} = \boldsymbol{E s_\alpha}(t) = (\boldsymbol{P_\alpha^T \Gamma_\alpha^T \Sigma_{\eta\eta}^{-1} \Gamma_\alpha P_\alpha} + \boldsymbol{L^T L})^{-1} \boldsymbol{P_\alpha^T \Gamma_\alpha^T \Sigma_{\eta\eta}^{-1} s_\alpha}(t) \tag{11}$$

We define a matrix $\boldsymbol{P_c^i}$ as the cropping matrix, which extracts the wave-front in the direction of the center of the GS asterism from the reconstructed phase distortion $\hat{\boldsymbol{\phi}}_{\boldsymbol{i}}$ of the i-th turbulent layer.

$$\hat{\boldsymbol{\phi}}^{\boldsymbol{i}}_{\boldsymbol{c}}(t) = \boldsymbol{P^i_c} \hat{\boldsymbol{\phi}}_{\boldsymbol{i}}(t). \tag{12}$$

where $\hat{\boldsymbol{\phi}}^{\boldsymbol{i}}_{\boldsymbol{c}}(t)$ is the wave-front at time t extracted from i-th turbulence layer. Before computing the temporal correlation, the extracted wave-front is converted into the slope by a discrete phase-to-slope operator $\boldsymbol{\Gamma_c}$.

$$\hat{\boldsymbol{s}}^{\boldsymbol{i}}_{\boldsymbol{c}}(t) = \boldsymbol{\Gamma_c} \hat{\boldsymbol{\phi}}^{\boldsymbol{i}}_{\boldsymbol{c}}(t), \tag{13}$$

where $\hat{\boldsymbol{s}}^{\boldsymbol{i}}_{\boldsymbol{c}}(t)$ is a reconstructed slope vector corresponding to a phase distortion of i-th atmospheric turbulence layer in the direction of the center of the GS asterism at time t. A peak of a slope correlation is sharper than the peak of a wavefront correlation, and can be detected easier than the peak of the wavefront correlation.

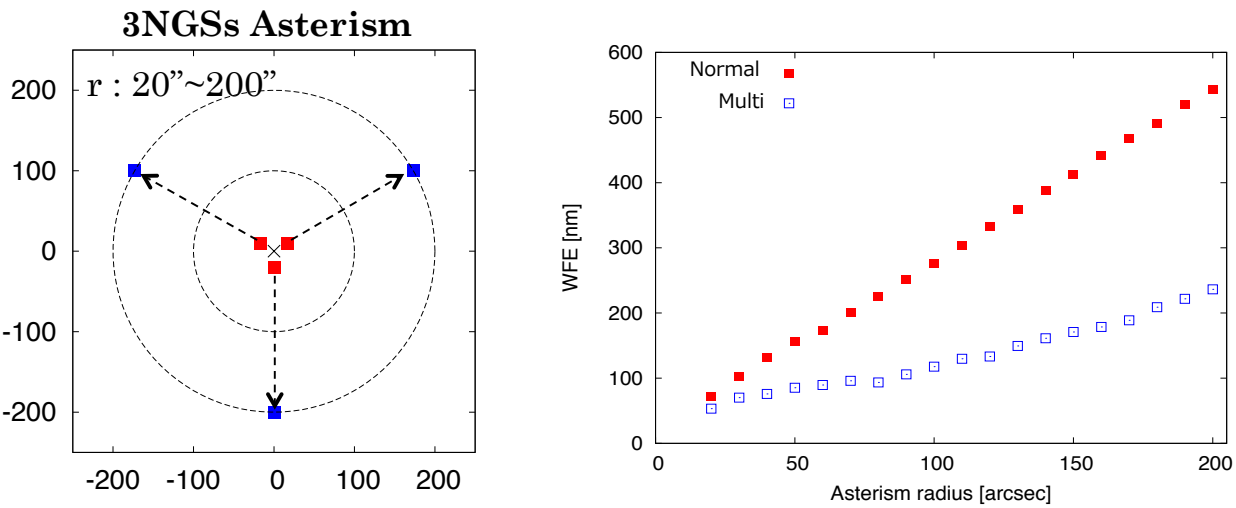

Figure 1. Left: Asterism of three GSs for the analytical evaluation. The radius of the asterism is set to from 20 arcseconds to 200 arcseconds. Right: The residual wavefront error computed with Eq. (15) as a function of the radius of the asterism. The red plots indicates the result of the single time-step reconstructor and the blue plots are the result of the multi-time step resonctructor.

Temporal correlation of the reconstructed slope at i-th turbulence layer can be computed as,

$$T^{[i]}_{xx}(\delta p, \delta q, \delta t) = \frac{\left\langle \sum_{p,q} \hat{s}^{x,i}_{c\ p,q}(t) \hat{s}^{x,i}_{c\ p+\delta p,q+\delta q}(t+\delta t) \right\rangle}{N(\delta p, \delta q)}. \tag{14}$$

where δt is the time delay for the temporal correlation, (p, q) is a index of the WFS subaperture in x and y direction, respectively, and $(\delta p, \delta q)$ is a spatial separation between two subapertures. The temporal correlation map $\boldsymbol{T^{[i]}_{xx}}$ can be obtained by computing Eq. (14) for all possible pairs of δp and δq. The correlation for y-direction slope is represented as similar to Eq. (14). In order to increase signal to noise, the correlations of x and y-direction slopes are averaged, $\boldsymbol{T^{[i]}} = (\boldsymbol{T^{[i]}_{xx}} + \boldsymbol{T^{[i]}_{yy}})$.

The movement of the correlation peak on the correlation map $\boldsymbol{T^{\mathbf{obs}[i]}}$ with δt corresponds to the wind speed and direction of ith turbulence layers. We use the centroid algorithm to detect the peak. When a subaperture size of SH-WFS is $d_{\rm sa}$ and the peak position is $(\delta p, \delta q)$, the wind speed is computed by $v_x = d_{\rm sa}\delta u/\delta t$ and $v_y = d_{\rm sa}\delta v/\delta t$. By computing v_x and v_y and averaging it over different δt, the wind speed and direction at each altitude can be estimated.

3. ANALYTICAL EVALUATION

The tip-tilt removed tomographic error in direction $\boldsymbol{\beta}$ is defined as

$$\sigma^2_{\boldsymbol{\beta},\rm tomo} = \frac{\mathbf{Tr}\left[\boldsymbol{R}(\boldsymbol{P_\beta} - \boldsymbol{E_\beta}\boldsymbol{\Gamma_\alpha}\boldsymbol{P_\alpha})\boldsymbol{\Sigma_{\phi\phi}}(\boldsymbol{P_\beta} - \boldsymbol{E_\beta}\boldsymbol{\Gamma_\alpha}\boldsymbol{P_\alpha})^T\boldsymbol{R}^T\right]}{n_p} + \frac{\mathbf{Tr}\left[\boldsymbol{R}\boldsymbol{E_\beta}\boldsymbol{\Sigma_{\eta\eta}}\boldsymbol{E_\beta^T}\boldsymbol{R}^T\right]}{n_p}, \tag{15}$$

where $\boldsymbol{R}$ is a matrix removing piston and tip-tilt modes from the residual wave-front and n_p is the number of phase point at the aperture plane. In this section, we evaluate the performance of the multi time-step tomographic reconstruction analytically with using Eq. (15).

The model for the analytical evaluation is as follows. We consider a MOAO system on a 30 m circular aperture telescope with three NGSs. The NGSs are put on a ring of a radius, which is a range of 20–200 arcseconds, indicated as the left panel of Fig. 1. We evaluate the tomographic error in the direction of the center of FoR. Fried parameter r_0 is 0.156 m and the outer scale is 30 m, which are typical value at Maunakea. The atmospheric

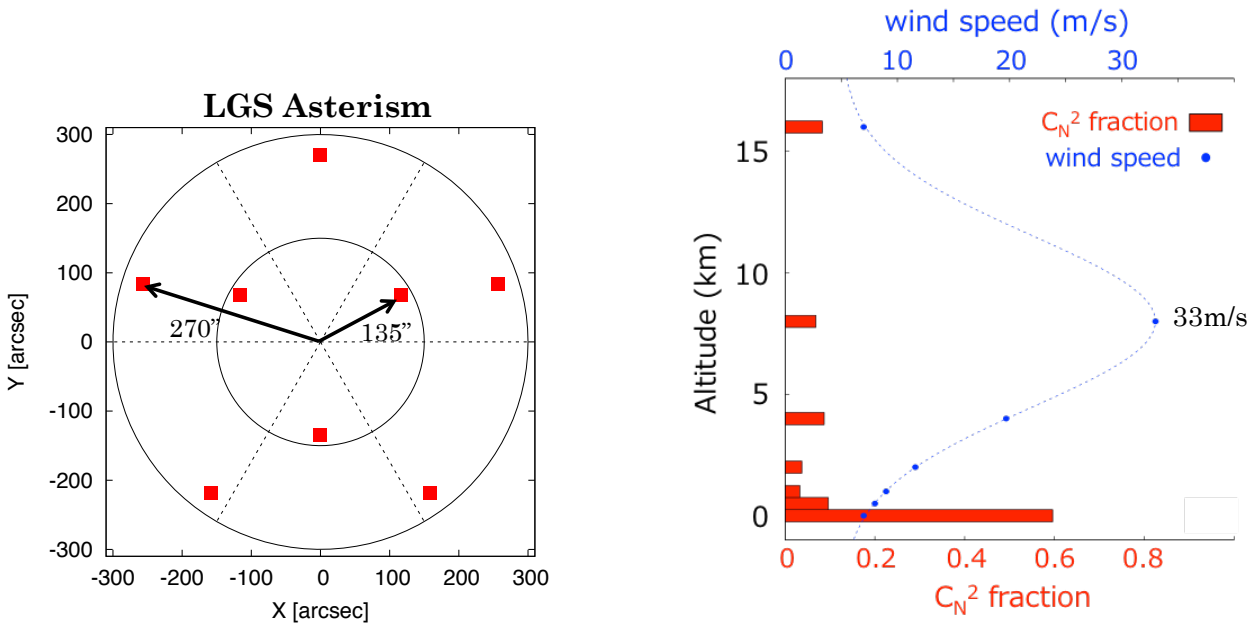

Figure 2. Left: Asterism of wight LGSs for the numrical simulation. The inner radius of the asterism is 135 arcseconds and the outer redius is 275 arcseconds. Right: C_N^2 profile and wind speeds used in the numerical simulation. The freid parameter, r_0, is 0.156m and the outer scale, L_0, is 30 m.

turbulence consists of three turbulence layers at 0 km, 5 km and 10 km. The C_N^2 fractions are [50 %, 25 %, 25 %], the wind speeds are [5 $\mathrm{m\,s^{-1}}$, 10 $\mathrm{m\,s^{-1}}$, 20 $\mathrm{m\,s^{-1}}$], and the wind directions are [90°, 0°, 0°] at 0, 5, and 10 km, respectively. The size of a WFS subaperture is 1 m on the aperture-plane and all subapertures have a same measurement noise with a variance of σ_η^2. The time difference Δt for the multi time-step reconstruction is set to 50 ms. The spatial sampling of discrete grids on the turbulence layers and the aperture-plane is 1 m. Over this chapter, the temporal lag error and the fitting error are not included in this analysis and we assume that we have the perfect knowledge of the turbulence altitudes, powers, and wind speeds and directions.

The result of the analytical valuation is shown in the right panel of Fig. 1. The tomographic error of the single time-step reconstructor, which is indicated by the red plots, increases rapidly with the radius of the asterism because of the increase of the *unoverlapped area*. While, the tomographic error of the multi time-step reconstruction increases mildly with the radius of the asterism compared with the tomographic error of the single time-step reconstructor since the multi time-step reconstructor reduces the *unoverlapped area* by using the measurements at both of the current and previous time-steps. The tomographic error of the multi time-step reconstruction at the asterism radius of 200 arcseconds is corresponding to the tomographic error of the single time-step reconstructor at the asterism radius of 80 arcseconds. Although this result is based on the optimal condition, where the turbulence altitudes, powers, and wind speeds and directions are given and the turbulence follows the frozen flow assumption, the multi time-step reconstructor has a possibility to reduce the geometric error and expand the FoR size dramatically.

4. NUMERICAL SIMULATION

In this chapter, we show the results based on the numerical simulation with assuming an ELT-scale MOAO system and investigate the expected performance of the multi time-step reconstruction on the future ELTs. We assume a circular aperture with 30 m diameter. The MOAO system has a FoR of 10 arcminutes diameter and does the tomographic reconstruction with eight sodium LGSs at altitude of 90 km, which the asterism is shown in the left panel of Fig. 2. In general, the LGS is not sensitive to the tip-tilt and focus modes of the turbulence. In this simulation, however, we assume that we can measure the tip-tilt and focus modes of the phase distortion from the LGSs for simplicity. We use SH-WFSs with 60×60 subapertures and DMs with 60×60 elements. The

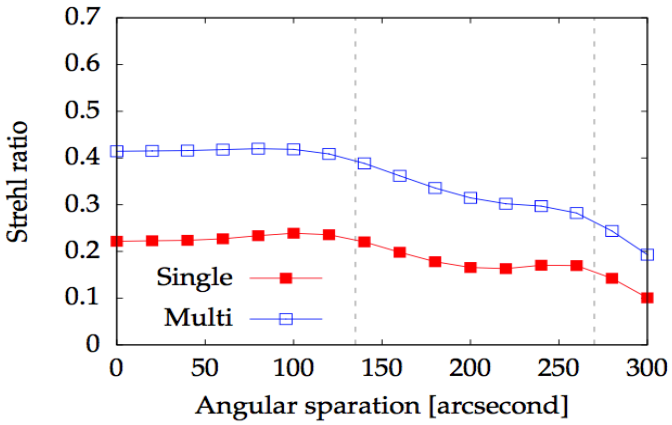

Figure 3. The SR values as a function of an angular separation from the center of the FoR. The red plots indicates the result of the single time-step reconstructor and the blue plots are the result of the multi-time step resonctructor.

spatial sampling of atmospheric turbulence is 0.05 m. The WFE is also evaluated with this spatial sampling to simulate the fitting error. We assume that the MOAO system is controlled with 800 Hz and there is two frames delay between the measurement by WFSs and correction by DMs, that is, 2.5 ms delay on a frame rate of 800 Hz. We assume the top of Maunakea as the observation site in the simulation and use a seven-layer model used in Andersen et al. (2012)[6] for the C_N^2 profile, shown in the right panel of Fig. 2. The turbulence is a 100% frozen flow turbulence. Fried parameter r_0 is 0.156 m and an outer scale is assumed to be 30 m. The assumed wind speeds and directions are also shown in the right panel of Fig. 2.

Fig. 3 shows the SR value as a function of the angular separation from the center of the FoR. While the SR value is 0.24 with the single time-step reconstructor at maximum, the multi time-step reconstructor with $\Delta t = 50$ ms can double the SR value over the FoR if the wind speeds and directions are known.

5. LABORATORY EXPERIMENT

Finally, we show the result of the laboratory experiment with RAVEN, which is a MOAO science and technical demonstrator. The RAVEN is a MOAO demonstrator installed and tested on the Subaru telescope at Maunakea.[7] The RAVEN can apply MOAO correction simultaneously for two science targets within a FoR of 2 arcminutes diameter by the tomographic reconstruction with 3 NGSs within a FoR of 3.5 arcminutes and 1 LGS attached to the Subaru telescope.[8] There are 4 open-loop SH-WFSs (OL-WFS) for 3 NGSs and 1 LGS in the RAVEN. All SH-WFSs consist of 10×10 subapertures, which has the diameter of 0.8 m on the aperture plane and a

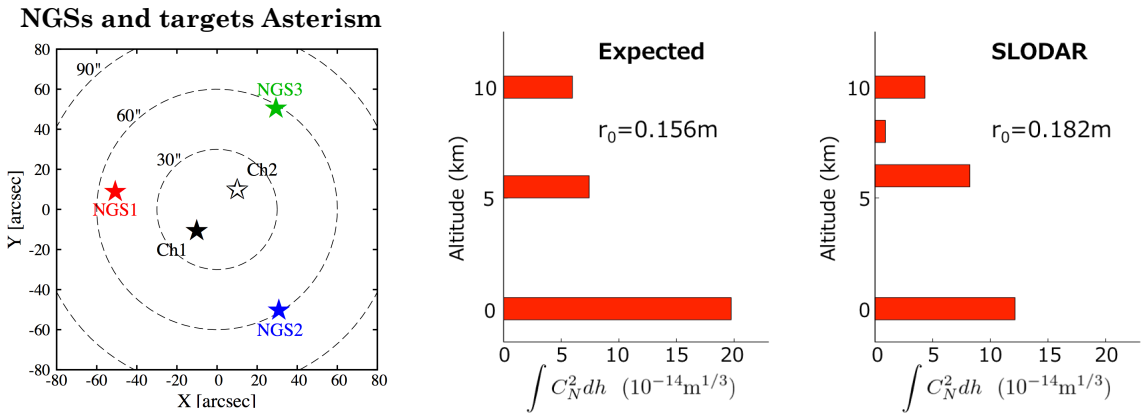

Figure 4. Left: Asterism of three GSs and science targets for the laboratory experiment with RAVEN. Middle: The C_N^2 profile generated by the CU in the RAVEN. Right: The C_N^2 profile estimated by SLODAR from the WFS measurements.

altitude [km]	wind x [$\mathrm{m\,s^{-1}}$]	wind y [$\mathrm{m\,s^{-1}}$]
0	0.0	5.68
5.5	6.0	0.0
10.5	17.0	0.0

Table 1. The wind speed at each altitude generated by the CU.

altitude [km]	wind x [$\mathrm{m\,s^{-1}}$]	wind y [$\mathrm{m\,s^{-1}}$]
0	0.1	5.0
6	6.3	0.1
8	8.6	-0.2
10	15.4	-0.6

Table 2. The estimated wind speed and direction from the measurement of the WFSs.

4.8 arcseconds FoV. The DMs are an ALPAO DM with 11×11 actuators. The RAVEN has a calibration unit (CU) on the optical bench, which simulates multiple GSs and science targets, atmospheric turbulence, and a telescope to calibrate and test the AO system.[9] The asterism of the GSs is shown in the left panel of Fig. 4. The atmospheric turbulences generated by the CU consist of three layers, which the C_N^2 profile is shown in the middle panel of Fig. 4. The designed wind speed and direction at each altitude is listed in Table 1.

The right panel of Fig. 4 is the C_N^2 profile estimated by Slope Detection and Ranging (SLODAR).[10–12] Although the total of the estimated r_0 is bit weaker than the designed value, the estimated C_N^2 fraction is consistent with the designed value. We use this profile in the tomographic reconstruction and the wind estimation. The estimated wind speed and direction at each altitude is shown in Table 2 and close to the designed value, in which the error of the wind speed is less than 2 $\mathrm{m\,s^{-1}}$at all altitudes.

The ensquared energy (EE) in 140 mas measured from the PSF images, which obtained in the laboratory experiment with RAVEN, are presented in Table 3. The multi time-step reconstruction is computed with the time difference, Δt, of 50 ms and the estimated wind speeds and directions. The improvement of the EEs due to the multi time-step reconstructor is 0.03–0.05. This result shows that the multi time-step works well in the laboratory experiment with the estimated wind information. It should be noted that the turbulence generated by the CU follows the frozen flow assumption, and that the effect of the boiling of the turbulence is not considered in this result.

6. CONCLUSION

We present the multi time-step reconstruction method to reduce the tomographic error due to the lack of information. In the analytical evaluation, we present that our tomographic reconstruction method is effective to reduce the tomographic error due to the lack of information. Then, we show the numerical simulation result of the tomographic reconstruction on multi-object adaptive optics (MOAO) system on the future extreme large telescope. The numerical simulation shows that the multi time-step reconstruction increases Strehl ratio (SR) over a field of regard of 10 arcminutes diameter by a factor of 2 if we know the wind speeds and directions. Finally, we present the laboratory experiment of our reconstruction method and the wind estimation method by using RAVEN, which is a MOAO demonstrator. We can successfully measure the wind speeds and directions in the laboratory experiment. Also, the multi time-step reconstructor can increase an ensquared energy (EE) in a 140 mas box by 0.03–0.05. It is noted that these results are assumed on the frozen flow assumption. In

Channel	single time-step reconstructor	multi time-step reconstructor
1	0.268	0.313
2	0.290	0.343

Table 3. The EE values in a 140 max box computed from the PSF images obtained in the labrotiry experiment.

order to understand and evaluate the effect of the boiling of the atmospheric turbulence, the on-sly experiment is necessary.

REFERENCES

[1] Beckers, J., "Increasing the size of the anisoplanatic patch with multiconjugate adaptive optics," *Proc. ESO conference* **4007**, 693–703 (1988).

[2] Hammer, F., Sayde, F., Gendron, E., Fusco, T., Burgarella, D., Cayatte, V., Conan, J., Courbin, F., Flores, H., Guinouard, I., Jocou, L., Lanon, A., Monnet, G., Mouhcine, M., Rigaud, F., Rouan, D., Rousset, G., Buat, V., and Zamkotsian, F., "The falcon concept: multi-object spectroscopy combined with mcao in near-ir," *Proc. ESO workshop* , 139 (2002).

[3] Correia, C., Jackson, K., Véran, J.-P., Andersen, D., Lardière, O., and Bradley, C., "Static and predictive tomographic reconstruction for wide-field multi-object adaptive optics systems," *J. Opt. Soc. Am. A* **31**, 101–113 (Jan 2014).

[4] Ellerbroek, B. L., "Efficient computation of minimum-variance wave-front reconstructors with sparse matrix techniques," *J. Opt. Soc. Am. A* **19**, 1803–1816 (Sep 2002).

[5] Gilles, L., Massioni, P., Kulcsár, C., Raynaud, H.-F., and Ellerbroek, B., "Distributed Kalman filtering compared to Fourier domain preconditioned conjugate gradient for laser guide star tomography on extremely large telescopes," *J. Opt. Soc. Am. A* **30**, 898–909 (May 2013).

[6] Andersen, D. R., Jackson, K. J., Blain, C., Bradley, C., Correia, C., Ito, M., Lardire, O., and Vran, J.-P., "Performance Modeling for the RAVEN Multi-Object Adaptive Optics Demonstrator," *Publications of the Astronomical Society of the Pacific* **124**(915), pp. 469–484 (2012).

[7] Lardire, O., Andersen, D., Blain, C., Bradley, C., Gamroth, D., Jackson, K., Lach, P., Nash, R., Venn, K., Vran, J.-P., Correia, C., Oya, S., Hayano, Y., Terada, H., Ono, Y., and Akiyama, M., "Multi-object adaptive optics on-sky results with Raven," *Proc. SPIE* **9148**, 91481G (2014).

[8] Hayano, Y., Takami, H., Oya, S., Hattori, M., Saito, Y., Watanabe, M., Guyon, O., Minowa, Y., Egner, S. E., Ito, M., Garrel, V., Colley, S., Golota, T., and Iye, M., "Commissioning status of Subaru laser guide star adaptive optics system," *Proc. SPIE* **7736**, 77360N (2010).

[9] Lavigne, J.-F., Lamontagne, F., Anctil, G., Wang, M., Tremblay, M., Lardire, O., Nash, R., Andersen, D., Savard, M., Ct, P., Bradley, C. H., and Chteauneuf, F., "Design and test results of the calibration unit for the MOAO demonstrator RAVEN," *Proc. SPIE* **8447**, 844754 (2012).

[10] Wilson, R. W., "SLODAR: measuring optical turbulence altitude with a ShackHartmann wavefront sensor," *Monthly Notices of the Royal Astronomical Society* **337**(1), 103–108 (2002).

[11] Butterley, T., Wilson, R. W., and Sarazin, M., "Determination of the profile of atmospheric optical turbulence strength from SLODAR data," *Monthly Notices of the Royal Astronomical Society* **369**(2), 835–845 (2006).

[12] Corts, A., Neichel, B., Guesalaga, A., Osborn, J., Rigaut, F., and Guzman, D., "Atmospheric turbulence profiling using multiple laser star wavefront sensors," *Monthly Notices of the Royal Astronomical Society* **427**(3), 2089–2099 (2012).